Published in final edited form as:

Proc IEEE Int Symp Biomed Imaging. 2012 May ; 2012: 418–421. doi:10.1109/ISBI.2012.6235573.

Automatic Sulcal Curve Extraction with MRF Based Shape Prior

Zhen Yang, **Aaron Carass**, and **Jerry. L. Prince**

Johns Hopkins University, 3400 N. Charles St., Baltimore, MD, USA 21218

Abstract

Extracting and labeling sulcal curves on the human cerebral cortex is important for many neuroscience studies, however manually annotating the sulcal curves is a time-consuming task. In this paper, we present an automatic sulcal curve extraction method by registering a set of dense landmark points representing the sulcal curves to the subject cortical surface. A Markov random field is used to model the prior distribution of these landmark points, with short edges in the graph preserving the curve structure and long edges modeling the global context of the curves. Our approach is validated using a leave-one-out strategy of training and evaluation on fifteen cortical surfaces, and a quantitative error analysis on the extracted major sulcal curves.

Index Terms

Sulcal curve extraction; cortical surface; Markov random field; shape prior; point set registration

1. Introduction

Cortical sulci are important structures on the cerebral cortex. They play a key role in identifying and measuring brain variability. Extracting and labeling sulci on human cortical surface is thus important in many neuroscience studies. Automatic extraction methods are typically used since manual delineation is too time consuming for the analysis of large populations.

Various approaches have been taken to detect sulcal curves or sulcal regions on the cortical mantle. Many methods extract pieces of sulcal curves or regions, without labeling them, by exploiting geometric information such as sulcal depth [1], isotropic geodesic distance maps [2]. To detect labeled sulcal curves, several works apply an extract and label strategy [3, 4], where sulcal curve pieces are first blindly extracted and then pruned and labeled by prior information learned from training data.

A deformable shape registration approach based on an Active Shape Model (ASM) was proposed in [5]. An initial set of sulcal curves deforms to match the sulcal geometric feature on a new brain while conforming to the shape statistics learned from the training data. However, due to the limited shape modes obtained from Principal Component Analysis (PCA), the method can only model a few major sulci which has relatively small variation across different brains.

In this paper, we follow the idea of a shape prior constrained deformable registration in [5]. Instead of a PCA based shape statistics, we use a Markov Random Field (MRF) to model the

joint distribution of shape points, which focuses on interactions between subsets of shape points, especially those in a geometric neighborhood. The low dimensionality of local statistics can be studied fully by limited training samples. In the rest of the paper, we first describe how to build the MRF model on shape points of sulcal curves and estimate MRF parameters from training samples, then we incorporate the MRF shape prior into the probabilistic based point set registration framework, and finally we demonstrate the effectiveness of the proposed method on 15 subjects with a leave-one-out strategy.

2. Method

Fig. 1 shows the fourteen major sulcal curves (on the left hemisphere) which we will be extracting. In order to study the shape statistics of sulcal curves in a common 2D manifold, the cortical surfaces of all training subjects are mapped to a unit sphere [6] and the MRF based shape statistics are computed from all the training shapes in this space. Given the cortical surface of a new subject with geometric features computed on every surface point, it is first mapped to the unit sphere, resulting in a subject's feature map on the unit sphere, then an initial shape is deformed to match the subject geometric features, and finally the resulting sulcal curves are projected back to the original cortical surface.

2.1. MRF model on shape points

In this work, the shape is formed by a set of sulcal curves S_i, $i = 1, 2,\ldots, N_s$, with each sulcal curve represented by a sequence of dense landmark points, $S_i=\{y_1^i, y_2^i, \ldots, y_{M_i}^2\}$, M_i. Let $Y=\cup_{i=1}^{N_s} S_i$ be the set of all the points that form the shape. We build the MRF model on point set Y described by an undirected graph $G = (Y, E)$, with each point being a node in the graph. The set of edges E encodes conditional dependences between the shape points. Assuming the Markovian property among the nodes, the Hammersley-Clifford theorem states that the joint probability distribution of any MRF can be written as a Gibbs distribution,

$$p(Y;\Theta)=\exp\left\{-\sum_{c\in C}\psi_c(Y_c;\Theta)-\log Z(\Theta)\right\}. \quad (1)$$

Where the product is over all cliques $c \in C$ in the graph. A clique is a subset of nodes in which every node is connected to every other node. Each $\psi_c(x_c; \Theta)$ is called a potential function and depends only on those random variables whose indices are in c. $Z(\Theta)$ is the partition function, and takes the form,

$$Z(\Theta)=\sum_{Y}\exp\left\{-\sum_{c\in C}\psi_c(Y_c;\Theta)\right\}.$$

2.2. Edge structure and potential functions

Though the shape of sulcal curves may vary greatly across different subjects, the spatial position of each sulci changes within a predictable range and the distances between neighboring sulci are relatively stable. We encode these observations in the MRF model by specifying potential functions on single-point cliques and multi-point cliques. We assume the single-point potential function follows a Gaussian distribution on the coordinates of landmark point, $\mathbf{y}_m$,

$$\psi_m(y_m)=\frac{1}{2}(\mathbf{y}_m-\bar{\mathbf{y}}_m)^T\sum_m^{-1}(\mathbf{y}_m-\bar{\mathbf{y}}_m).$$

Where $\bar{\mathbf{y}}_m$ and Σ_m are the mean and covariance of the coordinates.

Ideally a point is highly correlated with any other points within its spatial neighborhood and an edge can be created between the two points in the graph. However, this results in a over complicated graph with many redundant edges. To create a simpler graph, we selectively build two kinds of edges representing two kinds of correlations between shape points and specify potential functions for each edge set.

Short range correlations—Short range correlations are to preserve the smooth curve structure of each sulci. As shown in Fig. 2, short edges are created between sequential points in a curve and between two points separated by one point, forming the edge set E_s. We only consider potential functions on triangle cliques, the cliques formed by sequential three points in a curve. Let $c=\{y_1, y_2, y_3\}$ be a triangle clique in E_s and $\mathbf{y}_1, \mathbf{y}_2, \mathbf{y}_3$ be the coordinates of the three sequential points, the potential function is constructed as follows to penalize the second derivative of the curve,

$$\psi_c(y_1,y_2,y_3)=\frac{1}{2\sigma_c^2}\|\mathbf{y}_1-2\mathbf{y}_2+\mathbf{y}_3\|^2.$$

Long range correlations—Long range correlations are to preserve the distances between shape points in a spatial neighborhood. In order to generate isotropic edges for long range correlations, the shape points are partitioned into P non-overlapping downsampled versions of the original point set, Y_1, Y_2, …, Y_P and a Delaunay triangulation is carried out on each downsampled point set, generating triangular graph G_1, G_2, …, G_P with edge set E_1, E_2, …, E_P. The set of long edges is thus defined by $E_l=\cup_{p=1}^{P}E_p$, see Fig. 3. Again, only potential functions on triangle cliques are considered. For long range cliques, we assume the potential function follows a Gaussian distribution w.r.t the edge lengths of the triangle

$$\psi_c(y_1,y_2,y_3)=\frac{1}{2}(\mathbf{d}_c-\bar{\mathbf{d}}_c)^T\sum_c^{-1}(\mathbf{d}_c-\bar{\mathbf{d}}_c)$$

Where $\mathbf{d}_c = (\|\mathbf{y}_1 - \mathbf{y}_2\|, \|\mathbf{y}_2 - \mathbf{y}_3\|, \|\mathbf{y}_3 - \mathbf{y}_1\|)^T$. $\bar{\mathbf{d}}_c$ and Σ_c are the mean and covariance of the distances.

The joint distribution of all shape points in Eq. (1) can then be written as,

$$p(Y;\Theta)=\exp\left\{-\sum_{m=1}^{M}\psi_m(y_m;\Theta)-\sum_{c\in C_s}\psi_c(Y_c;\Theta)-\sum_{c\in C_l}\psi_c(Y_c;\Theta)-\log Z(\Theta)\right\}.$$

Where C_s is the set of all short range cliques and C_l is the set of all long range cliques. $\Theta = \{(\bar{\mathbf{y}}_m, \Sigma_m)|m = 1, 2, \ldots, M\} \cup \{\sigma_c|c \in C_s\} \cup \{(\bar{\mathbf{d}}_c, \Sigma_c)|c \in C_l\}$ is the set of MRF parameters.

2.3. MRF Parameter Estimation

Computing the maximum likelihood estimate of parameter set Θ is hard due to the intractability of the partition function $Z(\Theta)$. We take the approach of piecewise training [7], which independently trains the local potential function on each clique, afterwards combining the learned parameters into a single global model. For a clique c, $\Theta|_c$ is define as the restriction of Θ to c; that is, $\Theta|_c$ is the same as Θ, but with zeros in all entries that do not correspond to the clique c. The piecewise approximated log Gibbs distribution is defined as,

$$l_{\mathrm{PW}}(Y;\Theta)=\sum_{c\in C}[-\psi_c(Y_c)-\log Z(\Theta|_c)]. \quad (2)$$

Where $l_c(Y_c; \Theta|_c) = -\psi_c(Y_c) - \log Z(\Theta|_c)$ is the local log likelihood.

Since there are no common parameters between different cliques, the parameters $\Theta|_c$ and local partition function $Z(\Theta|_c)$ can be trained independently on each clique.

2.4. Deformable Registration with MRF Based Shape Prior

The point set registration framework in [8] is used for the shape deformable registration, which has shown to be both accurate and robust w.r.t initial positions and outlier points. Let X be the set of points sampled from the target image (geometric feature map of a subject cortical surface mapped onto the unit sphere). Y is the set of points to be deformed. The point set registration problem is considered as a probability density estimation problem, where the point set of deformable shape are the centroids of a Gaussian mixture model and the target image point set are data points. Given X, the optimal shape Y is computed by maximizing the posterior probability $p(Y|X)$ or equivalently, by minimizing the negative log likelihood function,

$$E(Y)=-\sum_{n=1}^{N}\log\Big(\sum_{m=1}^{M+1}\pi(m)p(x_n|m)\Big)-\lambda l_{\mathrm{PW}}(Y;\Theta),$$

where $l_{PW}(Y;\Theta)$ is the piecewise approximated log distribution of shape points Y in Eq. (2). $\pi(m)$ is the mixture weight and $p(x_n|m)$ are the component Gaussian distributions of both spatial coordinates and geometric features.

The optimization is solved by an Expectation-Maximization algorithm, and the initial shape Y_0 is the mean shape computed from the training shapes.

3. Experiments

We applied our method to the left hemisphere of 15 subjects from the Open Access Series of Imaging Studies (OASIS) [9] database. First, cortical surfaces are extracted from the MR images using the TOADS-CRUISE [10, 11, 12] software available from www.nitrc.org. Mean curvatures are computed on each subject's surface under different levels of inflation to form a feature vector at each point on the surface. The 14 major sulcal curves are manually delineated by a train rater on each subject surface. Leave-one-out experiments are carried out on the data set, using each subject as test subject and the remaining 14 subjects to train the MRF based shape prior. As shown in Fig. 4, the automatically extracted sulcal curves aligned well with the manually delineated ones.

In order to evaluate the extraction accuracy on each sulcal curve point, we compute two distances: $d_{am}(p_a)$, the distance from a point p_a on an automatically extracted sulcal curve to the corresponding manual traced sulcal curve and $d_{ma}(p_m)$ the manual traced to extracted ones. Fig. 5 shows that over 60% percent of the automatically extracted sulcal curve points are within 2mm of the manual traced points and over 80% within 5mm. We also plot the average d_{am} and d_{ma} over all subjects at each sulcal curve point, see Fig. 6. The main error comes from the end points of sulcal curves and regions that have high variability of sulcal shape or lack of geometric features.

To assess the performance on each sulcal curve, we compute the mean and max of d_{am} over all the points on a certain major sulcal curve, called respectively the average distance A_{am} and the Hausdorff distance, H_{am}, from the extracted curves to the manually traced ones. Similarly we have A_{ma} and H_{ma} from the manually traced to the extracted curves. Table 1 lists the four curve distances A_{am}, A_{ma}, H_{am} and H_{ma}, for each major sulci, averaged over all subjects. The average curve distance is around 2mm in both directions. Sylvian fissure, central sulcus and superior frontal sulcus obtained average distance of less than 2mm. The middle, inferior temporal sulcus and intraparietal sulcus have relatively large error due to the interruptions and shallowness of sulcal structure along the curve on the cortical surface. H_{am} and H_{ma} are relatively large because of the uncertainty in the end points of sulcal curves.

4. Conclusion

We propose a method for automatically extracting the major sulcal curves by registering a set of dense landmark points to the subject cortical surface. A Markov random field (MRF) is used to model the joint distribution of these landmark points with short edges in the graph preserving the curve structure and long edges modeling the global context of the curves. The method is applied to extract 14 major sulcal curves on the outer cortical surface and quantitative evaluation demonstrates good extraction accuracy. In future work, we would like

to further explore the graph structure of the shape points, such as the addition of more complicated long range interactions.

References

1. Rettmann ME, et al. Automated sulcal segmentation using watersheds on the cortical surface. NeuroImage. 2002; 15(2):329–344. [PubMed: 11798269]
2. Shi Y, et al. Hamilton–jacobi skeleton on cortical surfaces. IEEE Trans Med Imag. 2008; 27(5):664–673.
3. Shi Y, et al. Joint sulcal detection on cortical surfaces with graphical models and boosted priors. IEEE Trans Med Imag. 2009; 28(3):361–373.
4. Lyu I, et al. Spectral-based automatic labeling and refining of human cortical sulcal curves using expert-provided examples. NeuroImage. 2010; 52(1):142–157. [PubMed: 20363334]
5. Tao X, et al. Using a statistical shape model to extract sulcal curves on the outer cortex of the human brain. IEEE Trans Med Imag. 2002; 21(5):513–524.
6. Tosun D, et al. Mapping techniques for aligning sulci across multiple brains. Medical Image Analysis. 2004; 8(3):295–309. [PubMed: 15450224]
7. Sutton, C., et al. 21st Conference on Uncertainty in Artificial Intelligence. Citeseer; 2005. Piecewise training of undirected models.
8. Myronenko A, et al. Non-rigid point set registration: Coherent point drift. Advances in Neural Information Processing Systems. 2007; 19:1009.
9. Marcus DS, et al. Open Access Series of Imaging Studies (OASIS): Cross-Sectional MRI Data in Young, Middle Aged, Nondemented and Demented Older Adults. Jrnl of Cognitive Neuroscience. 2007; 19:1498–1507.
10. Carass A, et al. Simple paradigm for extra-cerebral tissue removal: Algorithm and analysis. NeuroImage. 2011; 56(4):1982–1992. [PubMed: 21458576]
11. Bazin PL, et al. Topology-Preserving Tissue Classification of Magnetic Resonance Brain Images. IEEE Trans Med Imag. 2007; 26(4):487–498.
12. Han X, et al. CRUISE: Cortical reconstruction using implicit surface evolution. NeuroImage. 2004; 23(3):997–1012. [PubMed: 15528100]

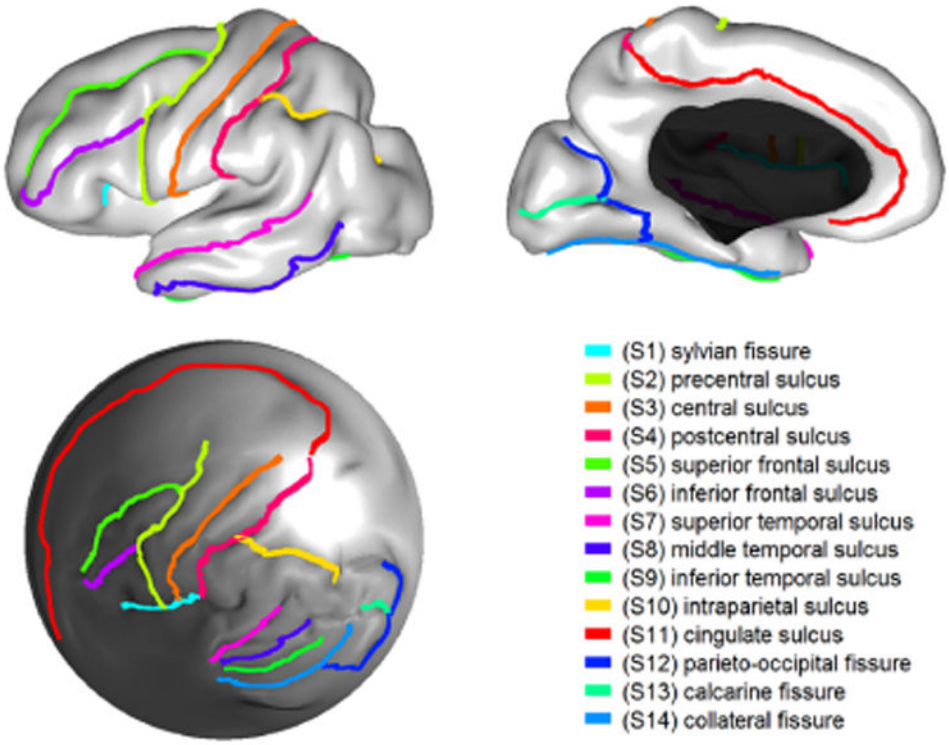

Fig. 1.
Fourteen major sulci on an inflated cortical surface and after mapping to the unit sphere.

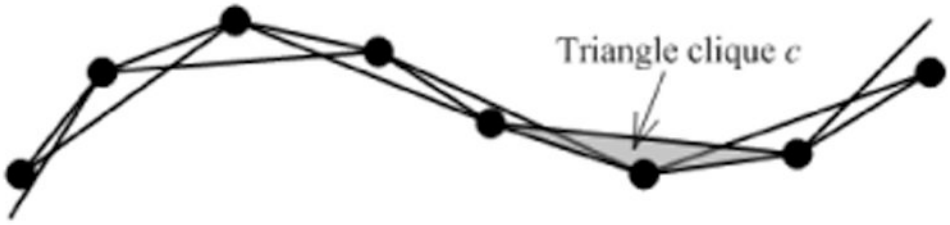

Fig. 2.
Short edges in the graph and the triangle cliques.

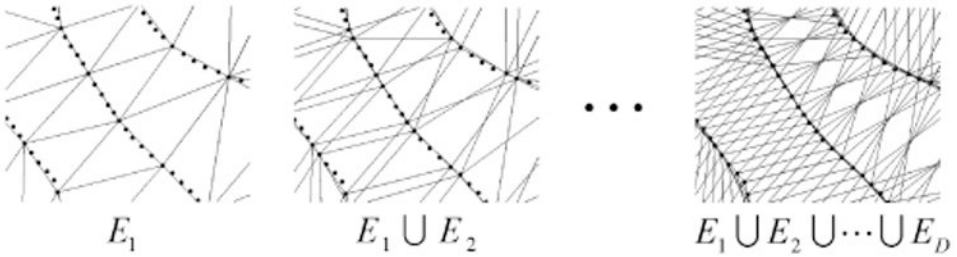

Fig. 3.

The set of long edges formed by accumulating triangularizations of downsampled shape points.

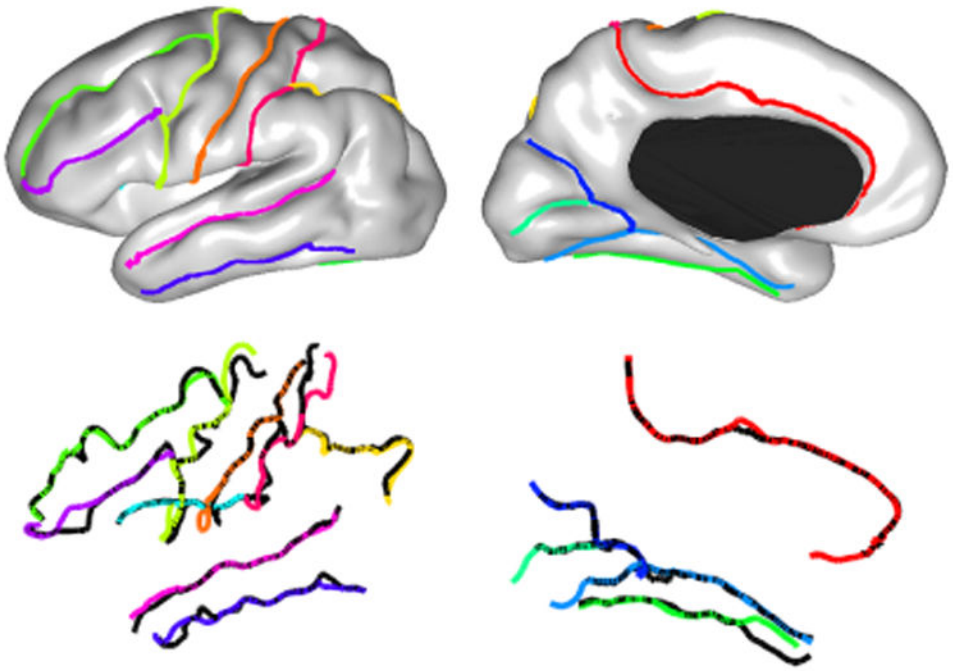

Fig. 4.

Example result on one subject. Top row: automatically extracted sulcal curves on the inflated surface. Bottom row: extracted sulcal curves overlayed with manual traced ones (shown in black).

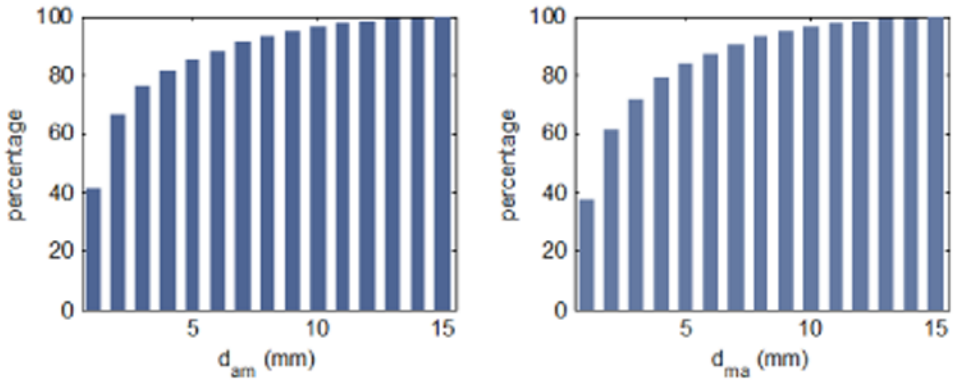

Fig. 5.

Cumulative histogram of d_{am} (left) and d_{ma} (right) over all sulci and all subjects.

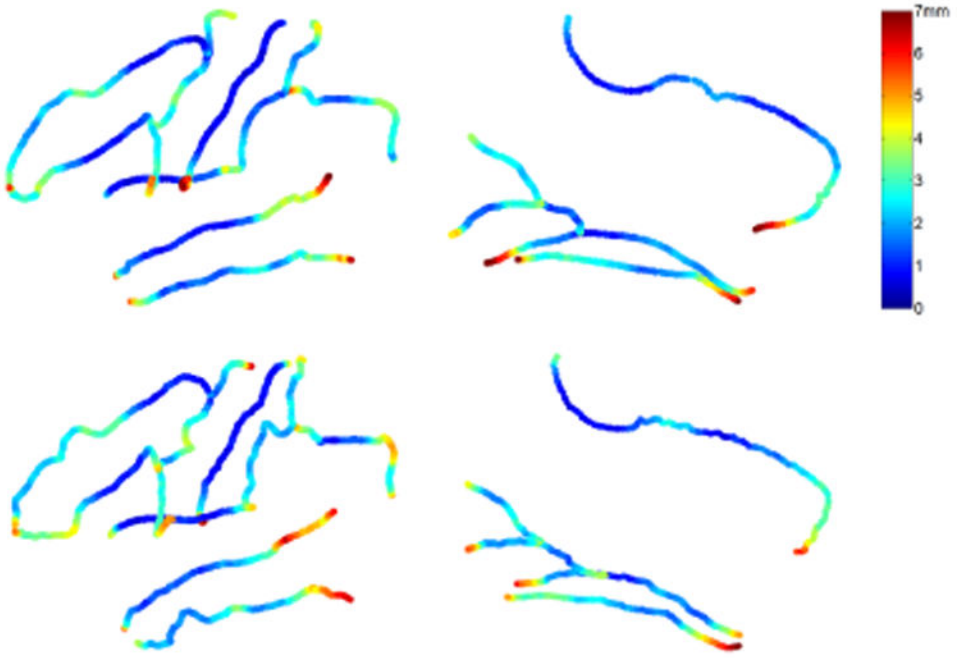

Fig. 6.
Point average d_{am} (top row) and d_{ma} (bottom row) over all subjects.

Table 1

Average and Hausdorff distances between an automatically extracted major sulcal curve and the manually traced one (unit:mm).

	S1	**S2**	**S3**	**S4**	**S5**	**S6**	**S7**
A_{am}	1.4	2.9	1.8	2.3	1.9	2.2	2.6
A_{ma}	1.5	3.0	2.0	2.7	2.1	2.7	3.1
H_{am}	5.2	9.2	8.4	7.9	7.9	8.4	10.4
H_{ma}	6.0	9.8	8.7	8.8	8.0	9.9	10.7
	S8	S9	S10	S11	S12	S13	S14
A_{am}	2.7	3.4	2.8	2.0	2.5	2.5	2.3
A_{ma}	2.9	3.1	3.0	2.1	2.6	2.7	2.3
H_{am}	11.4	10.5	9.3	10.7	9.4	7.2	9.3
H_{ma}	10.4	9.6	10.4	9.0	8.6	7.6	9.4